ISSN 1560-3547, Regular and Chaotic Dynamics, 2019, Vol. 24, No. 1, pp. 114–126. © Pleiades Publishing, Ltd., 2019.

The Dynamics of a Chaplygin Sleigh with an Elastic Internal Rotor

Vitaliy Fedonyuk* **and Phanindra Tallapragada****

Department of Mechanical Engineering, Clemson University, Clemson, SC 29634, U.S.A

Received November 11, 2018; revised January 02, 2019; accepted January 04, 2019

Abstract—In this paper the dynamics of a Chaplygin sleigh like system are investigated. The system consists a of a Chaplygin sleigh with an internal rotor connected by a torsional spring, which is possibly non-Hookean. The problem is motivated by applications in robotics, where the motion of a nonholonomic system is sought to be controlled by modifying or tuning the stiffness associated with some degrees of freedom of the system. The elastic potential modifies the dynamics of the system and produces two possible stable paths in the plane, a straight line and a circle, each of which corresponds to fixed points in a reduced velocity space. Two different elastic potentials are considered in this paper, a quadratic potential and a Duffing like quartic potential. The stiffness of the elastic element, the relative inertia of the main body and the internal rotor and the initial energy of the system are all bifurcation parameters. Through numerics, we investigate the codimension-one bifurcations of the fixed points while holding all the other bifurcation parameters fixed. The results show the possibility of controlling the dynamics of the sleigh and executing different maneuvers by tuning the stiffness of the spring.

MSC2010 numbers: 37J60, 70E55, 70K50

DOI: 10.1134/S1560354719010076

Keywords: nonholonomic systems, Chaplygin sleigh, passive degrees of freedom

1. INTRODUCTION

Mechanical systems with nonholonomic constraints are of significant interest in the design and control of mobile robots. Nonholonomic systems, such as spherical robots [1–3], skateboards and roller racers [4–10], and chained trailers [11–13], have been canonical problems where nonholonomic constraints play a key role in the dynamics and control of mobile robots. The dynamics and control of nonholonomic systems that have been commonly studied in relation to such robotics do not usually have a potential other than that due to gravity. The falling rolling disk is a classical example of such a system [14, 15]. The unicycle with a rider [16], the Chaplygin sleigh on an inclined surface [17] are a few other examples. On the other hand, the effect of elastic potentials on the dynamics of nonholonomic systems has received relatively little attention. Elastic potentials due to spring-like elements can play an important role in modifying the dynamics and control of mobile robots with nonholonomic constraints. For example, in [7] the motion of a wheeled vehicle with a linear spring was shown to asymptotically approach a straight line or a circle depending on the stiffness of the spring and a periodic applied moment. Associated with elastic potentials are passive or unactuated degrees of freedom. There is evidence that the animals use passive degrees of freedom with variable stiffness to control their motion or make it more efficient. Examples are the passive flapping of wings by insects to generate lift in hovering flight [18, 19], passive deformations of fish to extract energy from ambient wake in a stream [20, 21]. Experiments have also demonstrated that the maneuverability of swimming fish-like robots improves with passive tails, [22] and such fish like swimming robots have been shown to be subject to nonholonomic constraints [23–25]. These phenomena and experiments motivate an investigation of the role of passive degrees of freedom and

*E-mail: vfedony@g.clemson.edu

**E-mail: ptallap@clemson.edu

elastic potentials in the dynamics of nonholonomic systems, in particular, systems that are related to the Chaplygin sleigh.

In this paper, the dynamics of a modified Chaplygin sleigh consisting of an internal passive rotor joined by a torsional spring are investigated. The specific case of a rotor fastened at the center of mass of the sleigh is considered. An alternative physical interpretation of this modified Chaplygin sleigh is that the system consists of two rigid bodies, a head and a tail, which can pivot about each other and are connected by a torsional spring, with the tail being a Chaplygin sleigh, while the head is free to slide on the ground. Such a system without the presence of the elastic element was investigated in [26]. In this paper the same system with two cases of elastic potential functions is investigated, a quadratic potential due to a Hookean spring and a quartic potential due to a spring with a cubic nonlinearity. The stable motions of the system are analyzed and results of the numerical simulations of these are presented. It is shown that the addition of a spring leads to fixed points in the velocity space and that the limiting trajectory becomes periodic or a straight line. Unlike in [7, 10], we show that both motions, along a straight line and along a circle, can be stable for a given energy for the sleigh with a rotor if the elastic restoring force is allowed to be nonlinear. By adding an elastic degree of freedom the dynamics of the system can thus become more variegated without becoming chaotic. This work presents the utility of elastic joints in nonholonomic systems and provides a foundation to develop control algorithms for nonholonomic systems using passive degrees of freedom and elastic elements.

2. EQUATIONS OF MOTION

A schematic of the modified Chaplygin sleigh is shown in Fig. 1. The sleigh has a runner or a slender wheel at the rear that contacts the ground at the point P. The runner is assumed to be able to slide smoothly in its longitudinal direction but not in a transverse direction. The mass of the sleigh is denoted by m_c and the moment of inertia about its center by I_c. An internal rotor of mass m_r and moment of inertia I_r is hinged to the center of mass, C, of the sleigh, such that the rotor can rotate freely without any friction. The rotor and the Chaplygin sleigh are, however, connected by a torsional spring that resists a change in the relative motion of the two bodies. The configuration of the Chaplygin sleigh is parameterized by the location of its center of mass, (x, y), and its orientation θ, with respect to an inertial frame of reference. The relative angle between the two links is $\delta \in S^1$. The configuration space of the system is $Q = SE2 \times S^1$. The tuple (x, y, θ, δ) will be represented by $q = [q_1, q_2, q_3, q_4]^T$ for convenience. The body axes attached to point C are denoted by (X_b, Y_b).

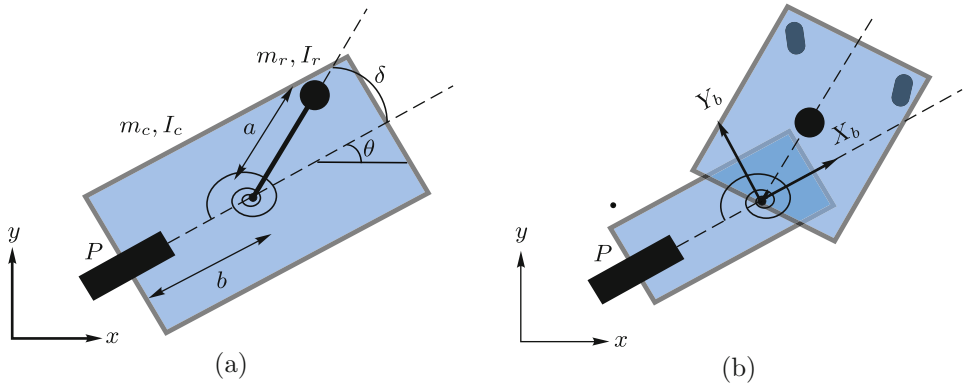

Fig. 1. The Chaplygin sleigh consists of a sleigh of mass m_c with a rear wheel or a sharp runner at distance b from the center of mass. The runner makes contact with the ground at point P. An internal rotor of mass m_r is attached to the center of the sleigh. The center of mass of the rotor is at distance a from the center of the sleigh. a) shows the second link represented as an internal rotor and b) shows the second link as an additional cart with casters.

The Lagrangian for the system is

$$\mathcal{L} = \frac{1}{2}\dot{q}^T \mathcal{M}(q)\dot{q} - \mathcal{V}(\delta), \tag{2.1}$$

where

$$\mathcal{M}(q) = \begin{bmatrix} m & 0 & -m_r\, a \sin(\delta+\theta) & -m_r\, a \sin(\delta+\theta) \\ 0 & m & m_r\, a \cos(\delta+\theta) & m_r\, a \cos(\delta+\theta) \\ -m_r\, a \sin(\delta+\theta) & m_r\, a \cos(\delta+\theta) & m_r\, a^2 + I_c + I_r & m_r\, a^2 + I_r \\ -m_r\, a \sin(\delta+\theta) & m_r\, a \cos(\delta+\theta) & m_r\, a^2 + I_r & m_r\, a^2 + I_r \end{bmatrix},$$

where $m = m_c + m_r$ is the total mass of the sleigh. The function $\mathcal{V}(\delta) = k_1\delta^2 + k_2\delta^4$ is the potential energy of the spring. The system must also satisfy a nonholonomic constraint that the rear wheel or runner is not allowed to slip in the transverse (Y_b) direction, i. e.,

$$\mathcal{W}(q)\dot{q} = 0, \tag{2.2}$$

where

$$\mathcal{W}(q) = \begin{bmatrix} -\sin\theta & \cos\theta & -b & 0 \end{bmatrix} \tag{2.3}$$

with Pfaffian one form being

$$-\sin\theta dx + \cos\theta dy - b d\theta = 0. \tag{2.4}$$

The equations of motion of the Chaplygin sleigh can be derived using the Lagrange multiplier method. Such calculations for the Chaplygin sleigh can be found in [27, 28], and these can be extended to the case of the Chaplygin sleigh with a passive internal rotor. The Euler – Lagrange equations are

$$\frac{d}{dt}\left(\frac{\partial \mathcal{L}}{\partial \dot{q}_k}\right) - \frac{\partial \mathcal{L}}{\partial q_k} = \mathcal{W}_k \lambda, \tag{2.5}$$

where λ is the Lagrange multiplier and $\mathcal{W}_k$ is the coefficient of the one form dq_k in (2.4).

Straightforward calculations yield the Euler – Lagrange equations as

$$\begin{bmatrix} \mathcal{M} & -\mathcal{W}^T \\ \mathcal{W} & 0 \end{bmatrix} \begin{bmatrix} \ddot{q} \\ \lambda \end{bmatrix} = \mathcal{B}(q, \dot{q}), \tag{2.6}$$

where

$$\mathcal{B}(q,\dot{q}) = \begin{bmatrix} \mathcal{C}(q,\dot{q})\dot{q} \\ \dot{\mathcal{W}}\dot{q} \end{bmatrix} + \frac{\partial \mathcal{L}}{\partial q}.$$

Here $\frac{\partial \mathcal{L}}{\partial q}$ is a vector of partial derivatives of the potential terms. For the Chaplygin sleigh with an internal rotor, this takes the form of $\left[0, 0, 0, \frac{\partial \mathcal{L}}{\partial \delta}, 0\right]^T$, since the only potential force is the restoring force on the spring. The matrix $\mathcal{C}(q,\dot{q})$ contains elements $c_{jk} = \sum_{i=1}^{n} c_{ijk}\dot{q}_i$ where c_{ijk} are the Christoffel symbols of the first kind computed as $c_{jk} = \sum_{i=1}^{n} \frac{1}{2}\left(\frac{\partial \mathcal{M}_{kj}}{\partial q_i} + \frac{\partial \mathcal{M}_{ki}}{\partial q_j} - \frac{\partial \mathcal{M}_{ij}}{\partial q_k}\right)\dot{q}_i$. For (2.5) this system becomes

$$\mathcal{B}(q,\dot{q}) = \begin{bmatrix} m_r\, a \cos(\delta+\theta)\,\dot{\delta}^2 + 2\, m_r\, a \cos(\delta+\theta)\,\dot{\delta}\dot{\theta} + m_r\, a \cos(\delta+\theta)\,\dot{\theta}^2 \\ m_r\, a \sin(\delta+\theta)\,\dot{\delta}^2 + 2\, m_r\, a \sin(\delta+\theta)\,\dot{\delta}\dot{\theta} + m_r\, a \sin(\delta+\theta)\,\dot{\theta}^2 \\ 0 \\ -4\, k_2\, \delta^3 - 2\, k_1\, \delta \\ \cos(\theta)\,\dot{\theta}\dot{x} + \sin(\theta)\,\dot{\theta}\dot{y} \end{bmatrix}. \tag{2.7}$$

The fifth equation of (2.6) is obtained by differentiating the nonholonomic constraint with respect to time. This is needed to complete the system in this form and solve for the velocities. In our formulation we eliminate the constraint force using Gaussian elimination in order to obtain the equations in matrix form useful for fixed points analysis. Let us define the body-fixed state vector $\xi = [u, \omega_1, \omega_2, \delta]^T$ where u is the velocity of P, $\omega_1 = \dot{\theta}$, and $\omega_2 = \dot{\delta}$. The velocities and accelerations of the tail may first be expressed in terms of u, ω_1 and θ as

$$\dot{x} = u\cos\theta - \omega_1 b\sin\theta \tag{2.8}$$

$$\dot{y} = u\sin\theta + \omega_1 b\cos\theta \tag{2.9}$$

and

$$\ddot{x} = \dot{u}\cos\theta - u\omega_1\sin\theta - \omega_1^2 b\cos\theta - \dot{\omega_1} b\sin\theta \tag{2.10}$$

$$\ddot{y} = \dot{u}\sin\theta + u\omega_1\cos\theta - \omega_1^2 b\sin\theta + \dot{\omega_1} b\cos\theta. \tag{2.11}$$

After substituting the above expressions into (2.6) and eliminating λ the following reduced equations are obtained:

$$\begin{bmatrix} \mathcal{M}_b & 0 \\ 0 & 1 \end{bmatrix} \dot{\xi} = \begin{bmatrix} \omega_1^2(m_r a\cos\delta + mb) + m_r a\omega_2^2\cos\delta + 2am_r\omega_1\omega_2\cos(\delta) \\ m_r ab\omega_2^2 sin\delta + 2m_r ab\omega_1\omega_2\sin(\delta) - u\omega_1(m_r a\cos(\delta) + mb) \\ -m_r au\omega_1\cos\delta - m_r ab\omega_1^2\sin(\delta) - 2k_1\delta - 4k_2\delta^3 \\ \omega_2 \end{bmatrix}, \tag{2.12}$$

where $\omega_1 = \dot{\theta}$, $\omega_2 = \dot{\delta}$, and δ is the angle made by the internal rotor with respect to the body X_b axis and $\mathcal{M}_b$ represents the locked inertia tensor:

$$\mathcal{M}_b = \begin{bmatrix} m & -m_r a\sin(\delta) & -m_r a\sin(\delta) \\ -m_r a\sin(\delta) & I_c + I_r + mb^2 + m_r a^2 + 2abm_r\cos(\delta) & m_r ab\cos\delta + I_r + m_r a^2 \\ -m_r a\sin(\delta) & m_r ab\cos\delta + I_r + m_r a^2 & I_r + m_r a^2 \end{bmatrix}. \tag{2.13}$$

3. FIXED POINTS OF THE ELASTIC CHAPLYGIN SLEIGH SYSTEM AND THEIR STABILITY

The block diagonal matrix $\begin{bmatrix} \mathcal{M}_b & 0 \\ 0 & 1 \end{bmatrix}$, hereafter denoted by $\mathbb{A}$, is invertible since the diagonal block $\mathcal{M}_b$ is the locked inertia tensor, a symmetric positive definite matrix. Denoting the right-hand side of (2.12) by $\mathbf{g}(\xi)$, the dynamical system (2.12) can be rewritten as

$$\dot{\xi} = \begin{bmatrix} \mathcal{M}_b & 0 \\ 0 & 1 \end{bmatrix}^{-1} \mathbf{g}(\xi) = \begin{bmatrix} \mathcal{M}_b^{-1} & 0 \\ 0 & 1 \end{bmatrix} \mathbf{g}(\xi) \equiv \mathbf{f}(\xi). \tag{3.1}$$

The fixed points of (3.1), denoted by $\xi^e = (u^e, \omega_1^e, \omega_2^e, \delta^e)$, satisfy $\mathbf{f}(\xi^e) = 0$, i. e., $\mathbb{A}^{-1}\mathbf{g}(\xi^e) = 0$. Since $\mathbb{A}^{-1}$ and $\mathcal{M}_b^{-1}$ are obviously invertible, the only solution to $\mathbb{A}^{-1}\mathbf{g}(\xi^e) = 0$ is the trivial solution $\mathbf{g}(\xi^e) = 0$. The last equation of (2.12), $\dot{\delta} = \omega_2$, implies $\omega_2^e = 0$, for any fixed point of (2.12). The total energy of the system, E, the sum of the kinetic energy of the sleigh, $\mathcal{T}(q, \dot{q})$, and the potential energy, $\mathcal{V}(q)$, stored in the elastic element is a constant, since the nonholonomic constraint force does not do any work. The velocity of the sleigh u can be eliminated in the dynamical system:

$$\begin{aligned} u(\omega_1, \omega_2, \delta; E) = \frac{1}{m}\Big(&\sin(\delta)\, am_r\,\omega_1 \pm \big((\sin(\delta))^2 a^2 {m_r}^2 {\omega_1}^2 - 2\cos(\delta)\, abm m_r\,{\omega_1}^2 \\ &- a^2 m m_r\,{\omega_1}^2 - b^2 m^2 {\omega_1}^2 - 2\,\delta^4 k_2\, m - I_r\, m{\omega_1}^2 - I_c\, m{\omega_1}^2 - 2\,\delta^2 k_1\, m + 2\,Em\big)^{1/2}\Big) \end{aligned} \tag{3.2}$$

Similarly, for a triplet ω_1^e, $\omega_2^e = 0$ and δ^e, a one-parameter set $u^e(E)$ exists. For instance, an inspection of (2.12) together with (3.2) shows that one set of fixed points is given by ($\omega_1^e = 0$, $\omega_2^e = 0$, $\delta^e = 0$) and

$$u^e = \sqrt{\frac{2E}{m}}. \tag{3.3}$$

The fixed points of the dynamical system (2.12) are nonisolated. The stability of such nonisolated fixed points can be analyzed by first reducing the dimension of (2.12).

If the four components of the vector field $\mathbf{f}(\xi)$ are denoted as $\mathbf{f}(\xi) = [f_1(\xi), f_2(\xi), f_3(\xi), f_4(\xi) = \omega_2]^T$, then the equations of motion reduced to a constant energy manifold are the last three equations of (3.1) with the velocity u replaced by (3.2)

$$\begin{bmatrix} \dot{\omega_1} \\ \dot{\omega_2} \\ \dot{\delta} \end{bmatrix} = \begin{bmatrix} f_2(E;\omega_1,\omega_2,\delta) \\ f_3(E;\omega_1,\omega_2,\delta) \\ \omega_2 \end{bmatrix} \equiv \mathbf{f}_R. \tag{3.4}$$

The fixed points of (3.4), denoted by $(\omega_1^e, \omega_2^e = 0, \delta^e)$, satisfy $\mathbf{f}_R\big(E(u^e);\omega_1,\omega_2,\delta\big) = 0$. Equivalently, the fixed points satisfy $\mathbf{g}_2\big(E(u^e);\omega_1^e,\omega_2^e,\delta^e\big) = 0$, $\mathbf{g}_2\big(E(u^e);\omega_1^e,\omega_2^e,\delta^e\big) = 0$ and $\omega_2^e = 0$. Every nonisolated fixed point ξ^e of the original dynamical system (3.1) leads to an isolated fixed point $(\omega_1^e, \omega_2^e = 0, \delta^e)$ on the manifold of constant energy, $E(u^e)$. To analyze the stability of these isolated fixed points, we linearize the system about $(\omega_1^e, \omega_2^e = 0, \delta^e)$. This allows us to determine whether the fixed point is stable or unstable by examining the eigenvalues of the Jacobian $\mathbf{Df}_R$ if these eigenvalues do not lie on the imaginary axis. Suppose the eigenvalues of the Jacobian $D\mathbf{f}_R(\omega_1^e, \omega_2 = 0, \delta^e)$ are denoted by $(\lambda_1, \lambda_2, \lambda_3)$ and

$$\sigma = \max_{i=1,2,3} \big(\mathrm{Re}(\lambda_i)\big),$$

then the fixed point $(\omega_1^e, \omega_2^e = 0, \delta^e)$ is stable if $\sigma < 0$ and unstable if $\sigma > 0$.

Due to the large parametric space in (3.4), the following scaling will be introduced:

$$\frac{m_c}{m} = \epsilon, \quad \frac{b}{a+b} = \epsilon, \quad I_c = Km_cb^2 = Kml^2\epsilon^3, \quad I_r = Km_ra^2 = Kml^2(1-\epsilon)^3, \tag{3.5}$$

where $l = a + b$. The spectral stability of the fixed points of (3.5) is investigated numerically for values $\epsilon \in (0, 1)$. The cases of $\epsilon = 0$ and $\epsilon = 1$ are singular, with either the head or the tail link becoming negligible. The stability analysis of fixed points of (3.4) shows dependence on the parameters ϵ and the total energy E, with bifurcations occurring as the parameters change. The following sections contain a detailed analysis of fixed points of (3.4). The fixed points and their stability are summarized in Table 1.

3.1. Motion Along a Line

The first category of equilibrium motion of the sleigh is motion along a straight line in the (x, y) plane (cases 1, 2, 5–7 and 8 in Table 1). Inspecting (2.12), these fixed points are such that $\omega_1^e = 0$, $\omega_2^e = 0$. The value of δ^e is given by the third equation of (2.12), $-2k_1\delta - 4k_2\delta^3$. When $k_1 > 0$ and $k_2 \geqslant 0$, this implies $\delta^e = 0$. When $k_1 < 0$ and $k_2 > 0$, however, three fixed points exist for $\delta^e \in \{0, \delta_1, \delta_2\}$, where δ_1 and δ_2 are the minima of the elastic potential, $\delta_{1,2} = \pm\sqrt{-\frac{k_2}{k_1}}$. These are the same fixed points for the reduced system (3.1).

A sample trajectory for the sleigh converging to a straight-line motion (case 1 with $\sigma < 0$) is shown in Fig. 2. In Fig. 2a the trajectory of the sleigh in the plane converges to a straight line whose slope is determined by the transient dynamics. The straight-line motion is indicated in Figs. 2b and 2c as the longitudinal velocity, $u(t)$, converges to the equilibrium value $u^e > 0$ and the angular velocities, ω_1 and ω_2, converge to zero.

Table 1. Fixed points of the dynamics (2.12) of the sleigh with various spring parameters. The fixed points are denoted by $(u^e, \omega_1^e, \omega_2^e, \delta^e)$ in the case of straight-line motion and by $(u^*, \omega_1^*, \omega_2^*, \delta^*)$ in the case of circular motion by the sleigh. Here $u^e(E)$ is given by (3.3), ω_1^* is given by (3.7), u^* is given by (3.8) and $\delta^* = \cos^{-1}\left(\frac{-mb}{m_r a}\right)$. In cases 1, 3, 7 and 9, where there are multiple fixed points, $(u^e, \omega_1^e, \omega_2^e, \delta^e)$, some of them are stable and some are unstable, which are indicated by (S/U). The fourth column shows the nature of the eigenvalues of the Jacobian of the reduced system (3.1). The notation employed is that each $a_{j,k} > 0$ corresponds to the jth case for $j = 1, 2, 3$ and $i = \sqrt{-1}$. The letter (U) indicates that the fixed point is unstable for all values of E and ϵ.

k_1, k_2	Case	Nonisolated Fixed Points	$\lambda\big(D\mathbf{f}_R(E(u^*); \omega_1^*, \omega_2^*, \delta^*)\big)$	Path
$k_1 > 0$ $k_2 \geqslant 0$	1	$u^e(E) > 0$, $\omega_1^e = 0$, $\omega_2^e = 0$, $\delta^e = 0$	$[-a_{1,1}, -a_{1,2}, -a_{1,3}]$ (S/U)	Line
	2	$u^e(E) < 0$, $\omega_1^e = 0$, $\omega_2^e = 0$, $\delta^e = 0$	$[a_{2,1}, a_{2,2} + a_{2,3}i, a_{2,2} - a_{2,3}i]$ (U)	Line
	3	$u^*(E) > 0$, $\omega_1^*(E)$, $\omega_2^* = 0$, δ^*	$[-a_{3,1}, \pm a_{3,2} - a_{3,3}i, \pm a_{3,2} + a_{3,3}i]$ (S/U)	Circle
	4	$u^*(E) < 0$, $\omega_1^*(E)$, $\omega_2^e* = 0$, δ^*	$[a_{4,1}, -a_{4,2} - a_{4,3}i, -a_{4,2} + a_{4,3}i]$ (U)	Circle
$k_1 < 0$ $k_2 > 0$	5	$u^e(E) > 0$, $\omega_1^e = 0$, $\omega_2^e = 0$, $\delta^e = 0$	$[a_{5,1}, -a_{5,2}, -a_{5,3}]$ (U)	Line
	6	$u^e(E) < 0$, $\omega_1^e = 0$, $\omega_2^e = 0$, $\delta^e = 0$	$[a_{6,1}, -a_{6,2}, a_{6,3}]$ (U)	Line
	7	$u^e(E) > 0$, $\omega_1^e = 0$, $\omega_2^e = 0$, $\delta^e \in \{\delta_1, \delta_2\}$	$[-a_{7,1} + a_{7,2}i, -a_{7,1} - a_{7,2}i, -a_{7,3}]$ (S/U)	Line
	8	$u^e(E) < 0$, $\omega_1^e = 0$, $\omega_2^e = 0$, $\delta^e \in \{\delta_1, \delta_2\}$	$[a_{8,1} + a_{8,2}i, a_{8,1} - a_{8,2}i, a_{8,3}]$ (U)	Line
	9	$u^*(E) > 0$, $\omega_1^*(E)$, $\omega_2^e = 0$, δ^*	$[-a_{3,1}, \pm a_{3,2} - a_{3,3}i, \pm a_{3,2} + a_{3,3}i]$ (S/U)	Circle
	10	$u^*(E) < 0$, $\omega_1^*(E)$, $\omega_2^e = 0$, δ^*	$[a_{10,1}, \pm a_{10,2} - a_{10,3}i, \pm a_{10,2} + a_{10,3}i]$ (U)	Circle
$k_1 = 0$ $k_2 = 0$	11	$u^e(E) > 0$, $\omega_1^e = 0$,$\omega_2^e = 0$, $\forall\delta$	$[0, 0, -a_{11,1}]$ (U)	Line
	12	$u^e(E) < 0$, $\omega_1^e = 0$, $\omega_2^e = 0$, $\forall\delta$	$[0, 0, a_{12,1}]$ (U)	Line
	13	$u^*(E) > 0$, $\omega_1^*(E)$, $\omega_2^e = 0$, δ^*	$[-a_{13,1}, a_{13,2} - a_{13,3}i, a_{13,2} + a_{13,3}i]$ (U)	Circle
	14	$u^*(E), 0$, $\omega_1^*(E)$, $\omega_2^e = 0$, δ^*	$[a_{14,1}, -a_{14,2} - a_{14,3}i, -a_{14,2} + a_{14,3}i]$ (U)	Circle

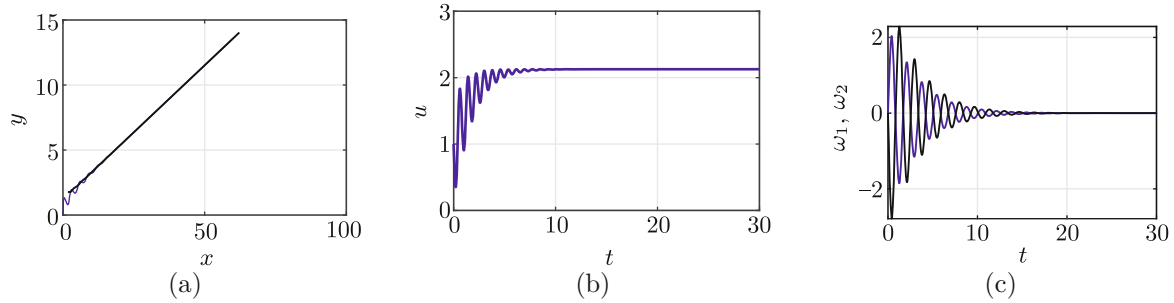

Fig. 2. Trajectory of the sleigh when $\epsilon = 0.3$ for case 1. Other parameters are $K = 1$, $k_1 = 1$, $k_2 = 0$ and $l = 1$. The (x, y) trajectory of the sleigh (blue) and the rotor (black) are shown in a), the longitudinal velocity in b), the angular velocities of the sleigh (blue) and rotor (black) in c).

When $u^e < 0$, in cases 2, 6 and 8, one of the eigenvalues of the Jacobian, $D\mathbf{f}_R(\omega_1^e, \omega_2^e, \delta^e)$, lies in the right half-plane, showing that these fixed points are unstable. In cases 1, 5 and 7, the equilibrium velocity of the sleigh is positive, $u^e > 0$. For case 5, when $k_1 < 0$ and $k_2 > 0$, the equilibrium state of $\delta^e = 0$ is unstable. In the remaining two cases, 1 and 7, the eigenvalues of $D\mathbf{f}_R(\omega_1^e, \omega_2^e, \delta^e)$ lie in the left half-plane for a range of values of ϵ and E, showing that fixed points are stable. However, these stable fixed points undergo bifurcations and the loss of stability as the parameter ϵ changes.

The fixed point in case 1 undergoes a Hopf bifurcation around $\epsilon = 0.707$. The real part of the three eigenvalues (one complex conjugate pair and a real eigenvalue) of $D\mathbf{f}_R$ evaluated at the fixed

point are shown in Fig. 3a. The fixed point changes stability only once at $\epsilon \approx \frac{1}{\sqrt{2}}$ in the range of $(0, 1)$ when the real part of the complex conjugate eigenvalues becomes positive. The complex conjugate eigenvalues are plotted in Fig. 3b showing a crossing from the left half to the right half of the complex plane when $\epsilon \approx \frac{1}{\sqrt{2}}$. Figure 3a shows these changing eigenvalues as the parameter ϵ is varying for an energy of $E = 1$. Numerical simulations show that the critical value of ϵ varies by less than 10^{-4} from 0.707 for $E = (0, 10^6)$.

In case 7, the stability of the fixed point undergoes three changes as the paramter ϵ varies in the interval $(0, 1)$.The real parts of the three eigenvalues of $D\mathbf{f}_R$ at the fixed point are plotted in Fig. 3c. For $\epsilon < 0.349$ the eigenvalues of $D\mathbf{f}_R$ are real with one of them being positive, with the fixed point being a rank-1 saddle. At $\epsilon \approx 0.349$ the fixed point changes stability from a rank-1 saddle to a stable node. A second bifurcation occurs at $\epsilon \approx 0.351$ when the stable node becomes a stable focus. Here two of the distinct real eigenvalues of $D\mathbf{f}_R$ transition to complex conjugates. This is shown in the inset figure in Fig. 3c. A third bifurcation occurs at $\epsilon \approx 0.698$ when the two complex conjugate eigenvalues cross the imaginary axis into the right half of the complex plane.

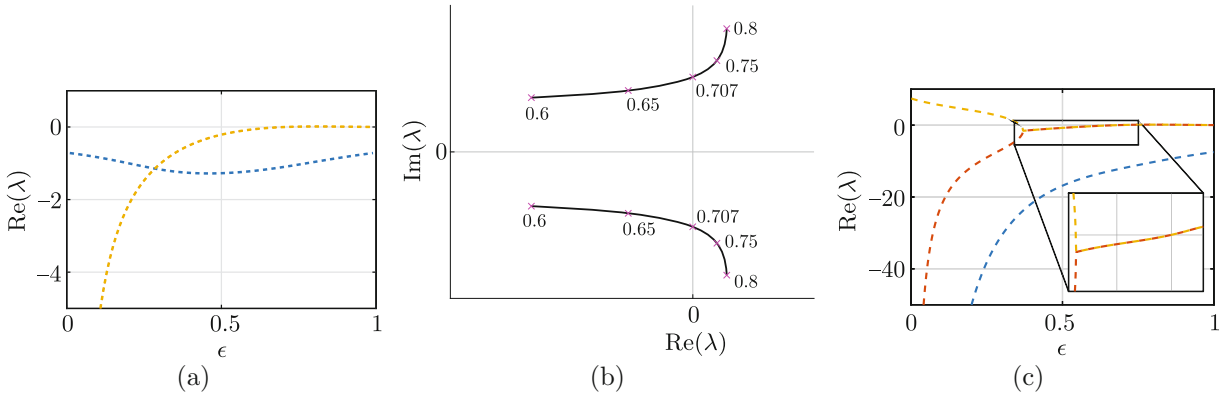

Fig. 3. a) Real parts of eigenvalues of $D(\mathbf{f}_R)$ for $\epsilon \in (0, 1)$ for case 1 with $k_1 = 1$ and $k_2 = 0$. b) A pair of eigenvalues crosses the imaginary axis as ϵ increases for case 1. The numbers on the plots indicate ϵ. c) Real parts of eigenvalues of $D(\mathbf{f}_R)$ for $\epsilon \in (0, 1)$ for case 7 with $k_1 = -7$ and $k_2 = 1$. Other parameters are $K = 1$, $E = 1$ and $l = 1$.

3.2. Motion on a Circle

The second category of equilibrium motion of the sleigh is that of a circle in the (x, y) plane. The fixed points of the dynamical system (2.12) that correspond to this motion are those of cases 3, 4, 9, 10, 13 and 14 in Table 1. For these cases the fixed points will be referred to as $\xi^* = (u^*, \omega_1^*, \omega_2^*, \delta^*)$. Inspecting (2.12), we see that $\omega_2^* = 0$ and $\delta^* = \pm\cos^{-1}\left(\frac{-mb}{m_r a}\right)$ cause all but the third equation to become zero. The existence of δ^* requires that $\frac{mb}{m_r a} < 1$, that is, the internal rotor has to have a larger mass and inertia than the mass of the main body. Due to this feature of the system a bifurcation occurs for all such fixed points such that the fixed point does not exist beyond a value of ϵ defined by

$$\frac{mb}{m_r a} = \frac{\epsilon}{(1-\epsilon)^2} = 1.$$

Using the fact that $\epsilon \in (0, 1)$, we find that this bifurcation occurs at $\epsilon = \frac{3}{2} - \frac{\sqrt{5}}{2} \approx 0.382$. In the alternate physical interpretation of the system, shown in Fig. 1b, this implies that the "tail" is smaller than the main body or the "head". Inspecting the third equation of (2.12), we find that equilibrium values u^* and ω_1^* satisfy

$$0 = -m_r a u^* \omega_1^* \cos\delta^* - m_r a b (\omega_1^*)^2 \sin(\delta^*) - 2k_1\delta^* - 4k_2\delta^{*3}. \tag{3.6}$$

The fixed point can be obtained by eliminating u^e from (3.6) using (3.2). This gives

$$\omega_1^* = \pm\sqrt{\frac{A \pm \sqrt{B}}{D}}, \tag{3.7}$$

where

$$\begin{aligned}
A &= am_r(\delta^4 k_2 + \delta^2 k_1 - E)\big(\cos(\delta)\big)^2 + 4\,\delta\,\sin(\delta)(\delta^2 k_2 + 1/2\,k_1)m_r a\cos(\delta) \\
&\quad + 4\,bm\delta\,\sin(\delta)(\delta^2 k_2 + 1/2\,k_1), \\
B &= \Big(a^2 {m_r}^2(\delta^4 k_2 - 4\,\delta^3 k_2 + \delta^2 k_1 - 2\,\delta\,k_1 - E)(\delta^4 k_2 + 4\,\delta^3 k_2 + \delta^2 k_1 + 2\,\delta\,k_1 - E)\big(\cos(\delta)\big)^2 \\
&\quad + (8\,am_r(\delta^4 k_2 + \delta^2 k_1 - E)\sin(\delta) - 32\,bm\delta\,(\delta^2 k_2 + 1/2\,k_1))\delta\,(\delta^2 k_2 + 1/2\,k_1)m_r a\cos(\delta) \\
&\quad - 16\,\delta\,\Big(-1/2\,abmm_r(\delta^4 k_2 + \delta^2 k_1 - E)\sin(\delta) + \delta\,(\delta^2 k_2 + 1/2\,k_1)\Big(-a^2 {m_r}^2 + a^2 mm_r \\
&\quad + m(mb^2 + I_c + I_r)\Big)\Big)(\delta^2 k_2 + 1/2\,k_1)\Big)\big(\cos(\delta)\big)^2, \\
D &= m_r((a^2 m_r + I_c + I_r)\big(\cos(\delta)\big)^2 + 2\,\cos(\delta)abm_r + mb^2)a.
\end{aligned}$$

Once ω_1^* is calculated, u^* can be calculated using (3.6) to get

$$u^* = -\frac{abm_r\omega_1^{*2}\sin(\delta^*) + 4\,k_2{\delta^*}^3 + 2\,k_1\delta^*}{am_r\omega_1^*\cos(\delta^*)}. \tag{3.8}$$

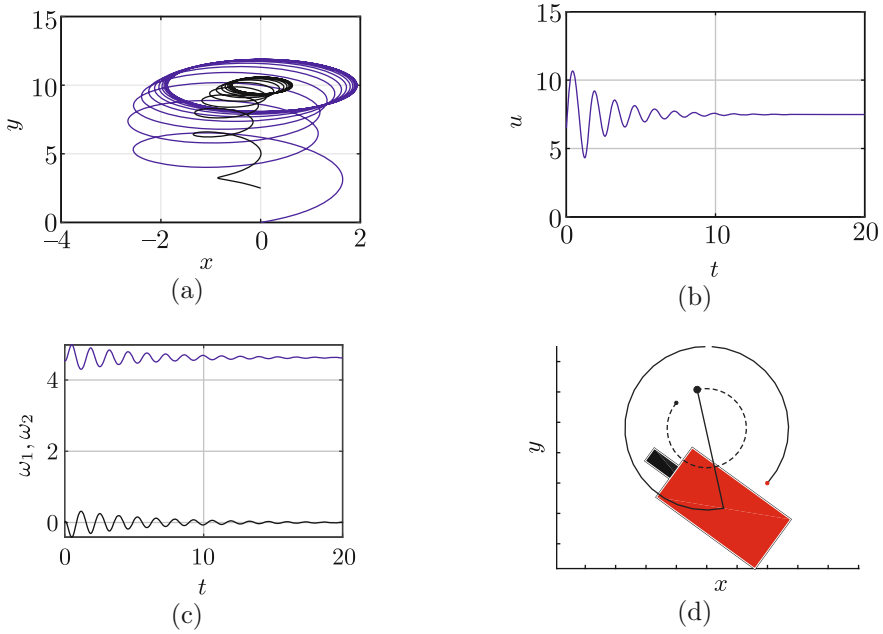

Fig. 4. The sleigh's trajectory converges to motion on a circle (case 9 with $\sigma < 0$). The parameters are $\epsilon = 0.35$, $K = 1$, $k_1 = -7$, $k_2 = 1$ and $l = 1$. The trajectory of the sleigh (blue) and the rotor (black) are shown in a), the longitudinal velocity in b), the angular velocities of the sleigh (blue) and rotor (black) in c). d) The sleigh traces out a circular path, in cases 3 and 9, with the relative angle between the rotor and the sleigh being constant, δ^*. The dashed line shows the path of the unbalanced rotor and the solid line shows the path of the sleigh.

In order to determine the path of the sleigh in the (x, y) plane, first note the fact that there is no relative motion between the rotor and the sleigh body, $\delta(t) = \delta^*$, and the sleigh moves with a constant velocity u^* and ω_1^*. Therefore, $\theta(t) = \omega_1^* t$ and we can substitute these values into (2.8)

and (2.9) to get

$$\dot{x} = A\cos(\omega_1^* t + \phi), \text{ and } \dot{y} = A\sin(\omega_1^t + \phi)$$

where

$$A = \sqrt{u^{*2} + b^2\omega_1^{*2}} \text{ and } \phi = \tan^{-1}(\frac{u}{b\omega_1^*}).$$

Integrating these we have

$$x - x_c = \frac{A}{\omega_1^*}\sin(\omega_1^* t + \phi), \text{ and}$$
$$y - y_c = -\frac{A}{\omega_1^*}\cos(\omega_1^* t + \phi).$$

Therefore, we get

$$(x - x_c)^2 + (y - y_c)^2 = \frac{A^2}{\omega_1^{*2}} = \left(\frac{u^*}{\omega^*}\right)^2 + b^2,$$

clearly the sleigh's path is a circle of radius $\sqrt{\left(\frac{u^*}{\omega^*}\right)^2 + b^2}$. An example of the simulation of the sleigh's motion in case 9 is shown in Fig. 4a: the trajectory of the sleigh converging to motion on a circle with the trajectory of the sleigh is shown in blue and that of the rotor in black. In this case $\omega_1 \to \omega^*$, $u(t) \to u^*$ and $\omega_2 \to 0$ (Fig. 4c). Consequently, the angle of the sleigh grows at a linear rate proportional to ω^* and $\delta \to \delta^*$. The equilibrium circular path of the sleigh is shown in 4d.

We find that for any given energy where the fixed point exists there are eight fixed points $\xi^* = (u^*, \omega_1^*, \omega_2^*, \delta^*)$ due to the positive and negative values of δ^* as well as the four solutions of (3.6) for (u^*, ω^*). As we vary the energy, the location of each such fixed point in the (u, ω_1) plane changes. Different (u^*, ω_1^*) are shown in Fig. 5a for energies ranging from 4.7 to 300 and a representative value of $\epsilon = 0.35$. The stability for these fixed points varies depending on the energy as well as the stiffness values k_1, k_2. This is seen in Fig. 5b where we fix the energy and vary the stiffness. Red regions are where the fixed point does not exist. The blue parameter regions are where the fixed point ξ^* exists but is unstable, and green regions are where the fixed point ξ^* is stable.

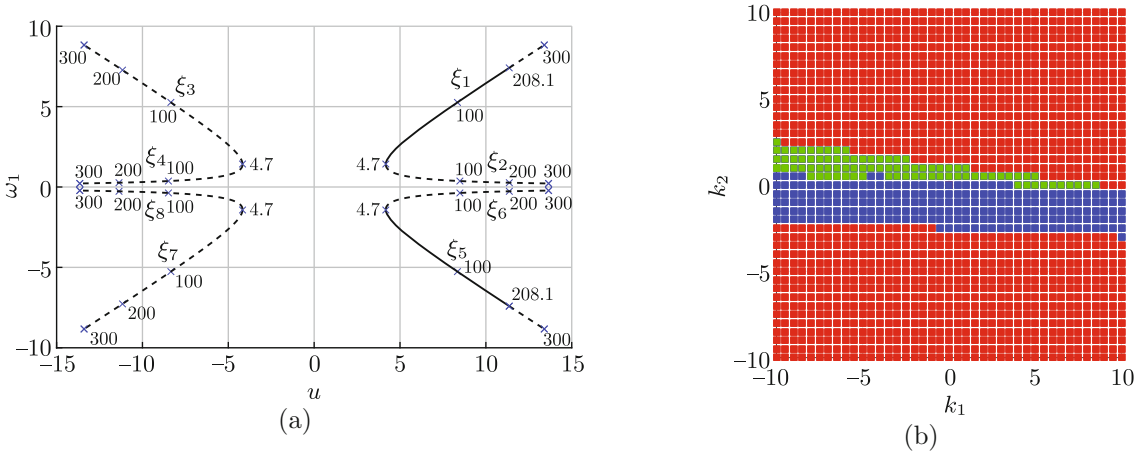

Fig. 5. a) Fixed points ξ^* (case 9) in the plane of u and ω_1 for energies ranging from 4.7 to 300. Here $\delta = \delta^*$, $\omega_2 = 0$, $k_1 = -7$, $k_2 = 1$, and $\epsilon = 0.35$. Solid lines indicate stable fixed points and dotted lines are unstable foci. These fixed points do not exist for energies lower than 4.7. Numbers on the plot indicate the energy for different points of interest. b) Existence and stability of the fixed point ξ^* for various values of k_1 and k_2 with a fixed energy of $E = 100$. Either the fixed point does not exist (red), it exists but is unstable (blue) or it exists and is stable (green).

As expected, the dynamics are symmetric about the ω_1 axis due to the symmetry in rotational dynamics. We can identify eight unique branches of fixed points $(\xi_1^*, \ldots, \xi_8^*)$ beginning from $E \approx 4.7$, four with $u^* > 0$ (case 9) and four with $u^* < 0$ (case 10). We can take $(\xi_1^*, \ldots, \xi_4^*)$ to be the four branches in the top half-plane ($\omega_1 > 0$). Let ξ_1^* refer to the branch with higher ω_1^* for $u^* > 0$ in the first quadrant of Fig. 5a and let ξ_2^* be the other branch with $u^* > 0$ in the first quadrant. Figure 5a shows the result of a numerical computation of the stability, and it can be seen that for the given parameters ξ_1^* is stable for low energies and becomes unstable for higher energies. For this value of $\epsilon = 0.35$ we also find that the branch ξ_2^* is unstable for all energies. The other two branches are unstable due to the negative value of u^*. In Fig. 6 we investigate the stability of ξ_2^* as a function of epsilon. We see in Fig. 6b that when we fix the energy and vary epsilon, ξ_2^* is stable for lower values of ϵ and becomes unstable after $\epsilon = 0.2$. A plot of $(\xi_1^*, \ldots, \xi_2^*)$ is shown in Fig. 6a for $\epsilon = 0.1$. We find that the general shape and stability of the branches changes as we vary ϵ.

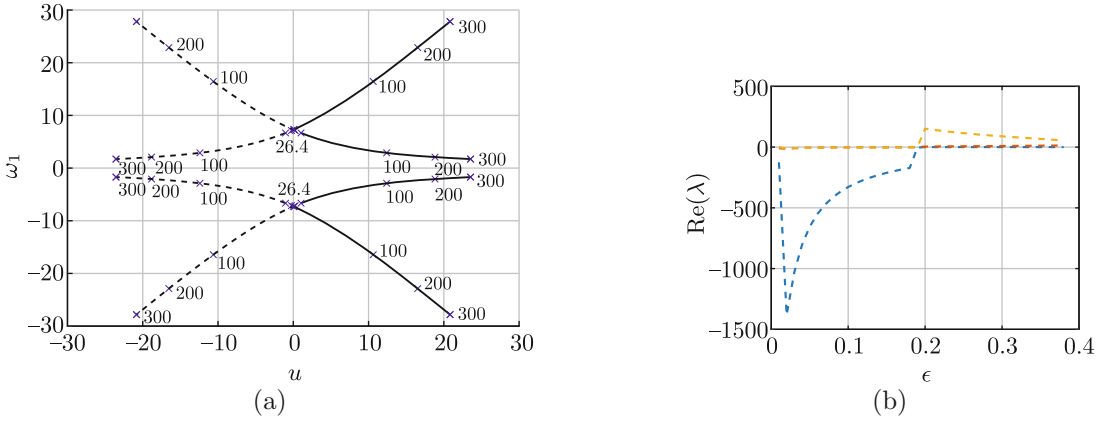

Fig. 6. a) Fixed points ξ^* (case 9) in the plane of u and ω_1 for energies ranging from 4.7 to 300. Here $\delta = \delta^*$, $\omega_2 = 0$, $k_1 = -7$, $k_2 = 1$ and $\epsilon = 0.1$. Solid lines indicate stable fixed points and dotted lines are unstable foci. These fixed points do not exist for energies lower than 4.7. Numbers on the plot indicate the energy for different points of interest. b) Real eigenvalues as a function of ϵ when the energy is $E = 700$.

Consider $k_1 = -7$, $k_2 = 1$ and take ξ_1^* in the first quadrant of Fig. 5a for an energy of $E = 100$. The eigenvalues of $D\mathbf{f}$ in this case are of the form $\lambda = [-a_{9,1}, -a_{9,2} - a_{9,3}j, -a_{9,2} + a_{9,3}j]$, therefore $\sigma < 0$ making ξ_1^* is a stable focus at this point. In Fig. 7a we see convergence to three different stable fixed points (one for case 7 and two fixed points ξ_1^* and ξ_5^* for case 9) for different initial conditions at three constant energies ($E = 80, 100, 120$). The fixed points are shown as a function of energy with black lines. The trajectories corresponding to case 7 converge to the $\omega_1 = 0$ axis and the trajectories converging to circular motion in case 9 are symmetrically placed around this fixed point at $\pm\omega_1^*$. All three fixed points are stable for the three energy levels shown. This figure shows that for any given energy cases 7 and 9 can both be stable simultaneously with asymptotic behavior of trajectories being dependent on initial conditions.

As the energy E increases, σ changes sign and ξ_1^* becomes locally unstable. The eigenvalues of $D\mathbf{f}$ cross the imaginary axis into the right half-plane at $E = 208.1$, (Fig. 7c). A stable limit cycle is formed around the unstable fixed point in a supercritical Hopf bifurcation. This is clearly shown in Fig. 7b, where we see how the fixed point ξ_1^* is at first a stable focus for energies of $E = 180$ and 200 and a stable limit cycle is formed around it for higher energies of $E = 220$ and $E = 240$. Note that the limit cycle is present in four dimensions. That is, ω_2 and δ also converge to periodic functions.

In order to identify other bifurcations the fixed point ξ^* may undergo, we vary $\epsilon \in (0, 0.382)$ and plot the complex eigenvalues of $D\mathbf{f}_R(\xi_1^*)$ of case 9 as well as a fixed point of the same energy for case 3. As ϵ is varied while holding the energy constant, the stability of these fixed points does not change for energies below $E \approx 520$. However, for higher energies, we find a double Hopf bifurcation where the complex eigenvalues cross the imaginary axis twice as ϵ is varied. This is seen in Figs. 8a and 8b where we vary ϵ for cases 3 and 9, respectively. We find that both cases undergo a similar bifurcation for an energy of $E = 700$. In case 9, the imaginary eigenvalues of $\mathbf{f}_R$ cross the imaginary

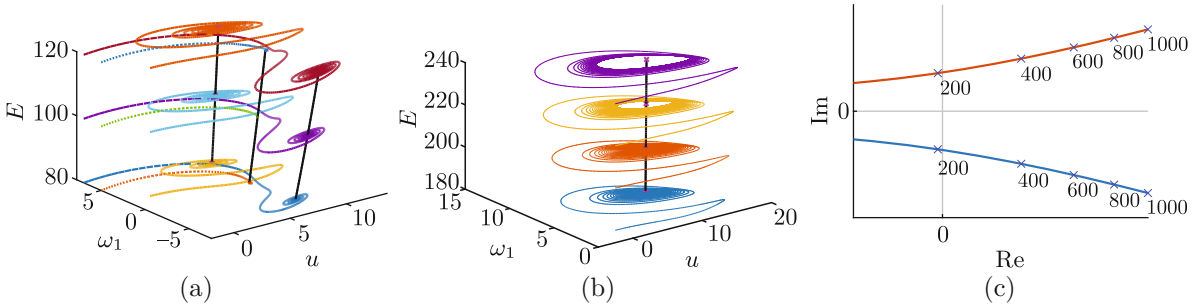

Fig. 7. a) Three stable trajectories of the sleigh corresponding to cases 7 and 9 with $\sigma < 0$ at energies of $E = 80$, $E = 100$, and $E = 120$. Initial conditions are chosen to lie on the corresponding energy level and the trajectory is plotted in the (u, ω_1, E) space. The fixed points as functions of energy are shown by the black lines. The trajectory where $\omega \to 0$ corresponds to case 7 and the trajectories to either side correspond to case 9 with symmetrically placed fixed points at $\pm\omega^*$ (ξ_1 and ξ_5 in Fig. 5a). b) The fixed point ξ_1^* goes from being stable to unstable and a stable limit cycle is formed around it (case 9 with transition from $\sigma < 0$ to $\sigma > 0$ as we vary energy). Convergence to the stable focus is shown for energies $E = 180$ and $E = 200$ and convergence to a stable limit cycle is seen for $E = 220$ and $E = 240$ c) Eigenvalues cross the imaginary axis and a supercritical Hopf bifurcation occurs at an energy of $E = 208.1$. Other parameters are $\epsilon = .35$, $k_1 = -7$, $k_2 = 1$, $K = 1$, $m = 1$, and $l = 1$.

axis from left to right near $\epsilon = 0.25$ and then in the opposite direction at $\epsilon = 0.36$. Before the first transition ξ^* is a stable focus. After the first crossing the point becomes unstable and a stable limit cycle is created around the fixed point, but as we increase ϵ further, the fixed point becomes a stable focus once again.

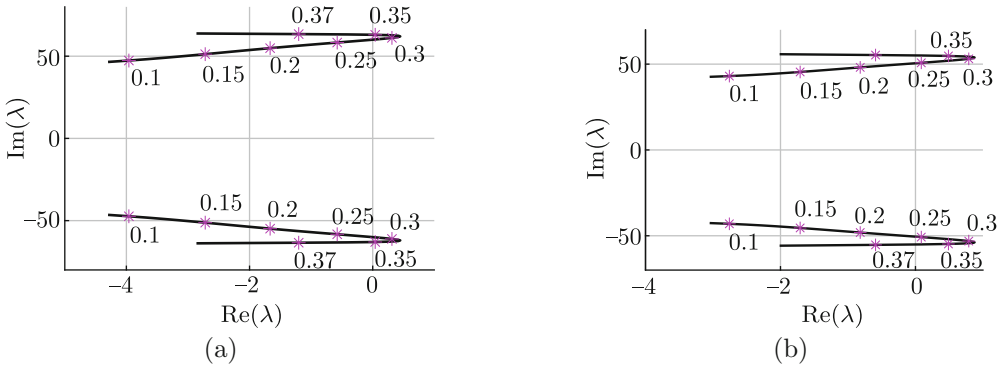

Fig. 8. Eigenvalues cross the imaginary axis as we vary ϵ for case 3 a) and case 9 b). The numbers on the eigenvalues show ϵ at selected values. In a) the energy is $E = 1000$ with $k_1 = 0$ and $k_2 = \frac{1}{4}$ and in b) the energy is $E = 600$ with $k_1 = -\frac{7}{2}$ and $k_2 = \frac{1}{4}$.

3.3. Dynamics of the System with no Elastic Element

If the spring element between the rotor and the sleigh's body is absent, the rotor is free to spin without any restoring torque. The fixed points for the case $k_1 = 0$ and $k_2 = 0$ correspond to cases 11–14 in Table 1. Two of these cases correspond to straight-line motion and two to circular motion. However, two of the eigenvalues of the $D\mathbf{f}_R$ are zero in case 11, where $u^e > 0$. Here a linearized analysis of stability is insufficient. However, extensive numerical simulations have shown that the fixed point in case 11 is unstable. The fixed points in the other cases, 12–14, are similarly unstable. The solutions to the dynamical system (2.12) converge to a chaotic attractor. For a thorough analysis of this case for a small rotor, we refer the reader to [26].

4. CONCLUSION

We have investigated the effect of a passive degree of freedom with an elastic potential on the Chaplygin sleigh, a well-known nonholonomic system. With just a passive internal rotor and no

elastic element the sleigh executes chaotic motion [26], while in the presence of an elastic element the sleigh can execute stable motion along a straight line or a circular path. In the reduced velocity space, such motions correspond to fixed points, which we have classified in this paper. These fixed points can undergo bifurcations and lose stability as the parameters of the system vary. Nevertheless, there exists a significant range of parameters where two kinds of stable motion are possible. The introduction of the passive elastic element produces a very rich variety of behaviors that are absent in the usual Chaplygin sleigh. The two primary types of stable motion of this modified system in the plane, straight lines and circles, can be used as the basis of motion planning and control for this system. We did not elucidate the full range of codimension-2 bifurcations associated with this system and instead presented results on codimension-1 bifurcations only for selected parametric values of stiffness and energy. An investigation of such bifurcations is left to future work.

REFERENCES

1. Joshi, V. A. and Banavar, R. N., Motion Analysis of a Spherical Mobile Robot, *Robotica,* 2009, vol. 27, no. 3, pp. 343–353.
2. Borisov, A. V., Kilin, A. A., and Mamaev, I. S., How to Control Chaplygin's Sphere Using Rotors, *Regul. Chaotic Dyn.,* 2012, vol. 17, nos. 3–4, pp. 258–272.
3. Karavaev, Yu. L. and Kilin, A. A., The Dynamics and Control of a Spherical Robot with an Internal Omniwheel Platform, *Regul. Chaotic Dyn.,* 2015, vol. 20, no. 2, pp. 134–152.
4. Hubbard, M., Lateral Dynamics and Stability of the Skateboard, *J. Appl. Mech.,* 1979, vol. 46, no. 4, pp. 931–936.
5. Ostrowski, J., Lewis, A., Murray, R., and Burdick, J., Nonholonomic Mechanics and Locomotion: The Snakeboard Example, in *Proc. of the IEEE Internat. Conf. on Robotics and Automation (San Diego, Calif., May 1994),* pp. 2391–2397.
6. Bloch, A. M., Krishnaprasad, P. S., Marsden, J. E., and Murray, R. M., Nonholonomic Mechanical Systems with Symmetry, *Arch. Rational Mech. Anal.,* 1996, vol. 136, no. 1, pp. 21–99.
7. Martynenko, Yu. G., The Theory of the Generalized Magnus Effect for Non-Holonomic Mechanical Systems, *J. Appl. Math. Mech.,* 2004, vol. 68, no. 6, pp. 847–855; see also: *Prikl. Mat. Mekh.,* 2004, vol. 68, no. 6, pp. 948–957.
8. Kremnev, A. V. and Kuleshov, A. S., Nonlinear Dynamics and Stability of the Skateboard, *Discrete Contin. Dyn. Syst. Ser. S,* 2010, vol. 3, no. 1, pp. 85–103.
9. Borisov, A. V., Mamaev, I. S., Kilin, A. A., and Bizyaev, I. A., Qualitative Analysis of the Dynamics of a Wheeled Vehicle, *Regul. Chaotic Dyn.,* 2015, vol. 20, no. 6, pp. 739–751.
10. Bizyaev, I. A., The Inertial Motion of a Roller Racer, *Regul. Chaotic Dyn.,* 2017, vol. 22, no. 3, pp. 239–247.
11. Murray, R. M. and Sastry, S. Sh., Nonholonomic Motion Planning: Steering Using Sinusoids, *IEEE Trans. Automat. Control,* 1993, vol. 38, no. 5, pp. 700–716.
12. Tilbury, D., Murray, R. M., and Sastry, S. Sh., Trajectory Generation for the n-Trailer Problem Using Goursat Normal Form, *IEEE Trans. Automat. Control,* 1995, vol. 40, no. 5, pp. 802–819.
13. Bravo-Doddoli, A. and García-Naranjo, L. C., The Dynamics of an Articulated n-Trailer Vehicle, *Regul. Chaotic Dyn.,* 2015, vol. 20, no. 5, pp. 497–517.
14. Neimark, Ju. I. and Fufaev, N. A., *Dynamics of Nonholonomic Systems,* Trans. Math. Monogr., vol. 33, Providence, R.I.: AMS, 1972.
15. Arnol'd, V. I., Kozlov, V. V., and Neĭshtadt, A. I., *Dynamical Systems 3,* Encyclopaedia Math. Sci., vol. 3, Berlin: Springer, 1988.
16. Zenkov, D. V., Bloch, A. M., and Marsden, J. E., The Lyapunov – Malkin Theorem and Stabilization of the Unicycle with Rider, *Systems Control Lett.,* 2002, vol. 45, no. 4, pp. 293–302.
17. Borisov, A. V. and Mamaev, I. S., The Dynamics of a Chaplygin Sleigh, *J. Appl. Math. Mech.,* 2009, vol. 73, no. 2, pp. 156–161; see also: *Prikl. Mat. Mekh.,* 2009, vol. 73, no. 2, pp. 219–225.
18. Dickinson, M. H., Lehmann, F.-O., and Sane, S. P., Wing Rotation and the Aerodynamic Basis of Insect Flight, *Science,* 1999, vol. 284, no. 5422, pp. 1954–1960.
19. Whitney, J. P. and Wood, R. J., Aeromechanics of Passive Rotation in Flapping Flight, *J. Fluid Mech.,* 2010, vol. 660, pp. 197–220.
20. Beal, D. N., Hover, F. S., Triantafyllou, M. S., Liao, J. C., and Lauder, G. V., Passive Propulsion in Vortex Wakes, *J. Fluid Mech.,* 2006, vol. 549, pp. 385–402.
21. Fish, F. E. and Lauder, G. V., Passive and Active Flow Control by Swimming Fishes and Mammals, *Annu. Rev. Fluid Mech.,* 2006, vol. 38, pp. 193–224.

22. Pollard, B. and Tallapragada, P., Passive Appendages Improve the Maneuverability of Fish-Like Robots, *IEEE/ASME Trans. Mechatronics,* 2018, accepted.
23. Tallapragada, P., A Swimming Robot with an Internal Rotor As a Nonholonomic System, in *Proc. of the American Control Conf. (ACC, Chicago, Ill., July 2015),* pp. 657–662.
24. Tallapragada, P. and Kelly, S. D., Integrability of Velocity Constraints Modeling Vortex Shedding in Ideal Fluids, *J. Comput. Nonlinear Dynam.,* 2016, vol. 12, no. 2, 021008, 7 pp.
25. Pollard, B., Fedonyuk, V., and Tallapragada, P., Limit Cycle Behavior and Model Reduction of an Oscillating Fish-Like Robot, in *Proc. of the ASME Dynamic Systems and Control Conference (Atlanta, Ga., Sept 30–Oct 3, 2018): Vol. 1,* Paper No. DSCC2018-9016, pp. V001T04A006, 7 pp.
26. Fedonyuk, V. and Tallapragada, P., Chaotic Dynamics of the Chaplygin Sleigh with a Passive Internal Rotor, *Nonlinear Dynam.,* 2019, vol. 95, no. 1, pp. 309–320.
27. Fedonyuk, V. and Tallapragada, P., The Stick-Slip Motion of a Chaplygin Sleigh with a Piecewise Smooth Nonholonomic Constraint, *J. Comput. Nonlinear Dynam.,* 2017, vol. 12, no. 3, 031021, 8 pp.
28. Tallapragada, P. and Fedonyuk, V., Steering a Chaplygin Sleigh Using Periodic Impulses, *J. Comput. Nonlinear Dynam.,* 2017, vol. 12, no. 5, 054501, 5 pp.